

Section 8

Development of and advances in ocean, sea-ice,
and wave modelling and data assimilation.

Hourly Analysis of Significant Wave Height by the UnRestricted Mesoscale Analysis System at NCEP

S. Flampouris¹, M. S. F. V. De Pondecá¹, J. Whiting¹, J. R. Carley², J.H.G.M. Alves³, R. Yang¹ & S. Levine³

¹IM Systems Group at NOAA/NCEP; ²NOAA/NCEP/EMC; ³Systems Research Group; College Park, MD, USA
Email: stylianos.flampouris@noaa.gov

Introduction

The National Centers for Environmental Prediction (NCEP) of NOAA provide weather guidance to the United States National Weather Service (NWS). The UnRestricted Mesoscale Analysis (URMA) is designed as an extension to the Real-Time Mesoscale Analysis System [1] to provide the most accurate, gridded analysis of near-surface sensible weather elements, cloud fields, and significant wave height (SWH) with a six-hour lag. The URMA products are disseminated to forecasting offices, serve as the *analysis of record* for the National Digital Forecast Database [2], and are used in calibrating the National Blend of Models [3]. Since version 2.6, implemented in December of 2018, the URMA has provided a SWH analysis for the Contiguous United States (CONUS) [4]. This paper explores the expansion of URMA for SWH to Alaska (AK), Hawaii (HI), and Puerto Rico (PR) – the OCONUS – domains, as well as the system upgrades in the next URMA generation, version 2.7.

URMA System for Significant Wave Height

URMA is a two-dimensional application of the community Gridpoint Statistical Interpolation (GSI) data assimilation system [5], which was recently upgraded to provide an analysis of SWH. The nominal spatial resolution of the analysis is 2.5 km for CONUS, HI, and PR, and it is 3 km for AK. SWH observations are currently assimilated from five satellites: Jason-2 and -3, Cryosat-2, Saral/Altika, and Sentinel-3; and also from in-situ SWH (buoys, drifters, and ships of opportunity). The background field is provided by the operational deterministic wave prediction system, known as multi_1, based on the WAVEWATCH III® model [6]. The preprocessing of the background is independent of the prediction system; and is based on the wgrib2 utility [7], which primarily involves interpolating and re-projecting the SWH background field on the appropriate URMA domain. Advantages of this upgrade include i) a significant reduction of the preprocessing time, by approximately ten times, and ii) the GSI can provide analysis of SWH with background fields from any wave model or blend of SWH predictions, even with different resolutions.

The default GSI background error properties were also calibrated for nearshore applications; the error variance is set to 0.4m^2 and the correlation length 150km. For the four URMA domains, both variance and correlation lengths were estimated locally and provided through external files. An analysis of monthly model prediction and buoy data for 2015 and 2016 provided the estimated values of the background error. The length of the temporal window of the analysis is 3 hours according to the estimated temporal decorrelation length and the real-time availability of the SWH observations.

Analysis of Significant Wave Height for OCONUS

The URMA was deployed and calibrated for the three URMA OCONUS domains. The analysis was verified regarding bias and Root Mean Square Error (RMSE). As expected, the error statistics of the analysis are significantly reduced in comparison with the error statistics of the background field, Figure 1. One limitation is the small number of observations, for instance for PR, there are only three permanent, nearshore buoys and no satellite coverage.

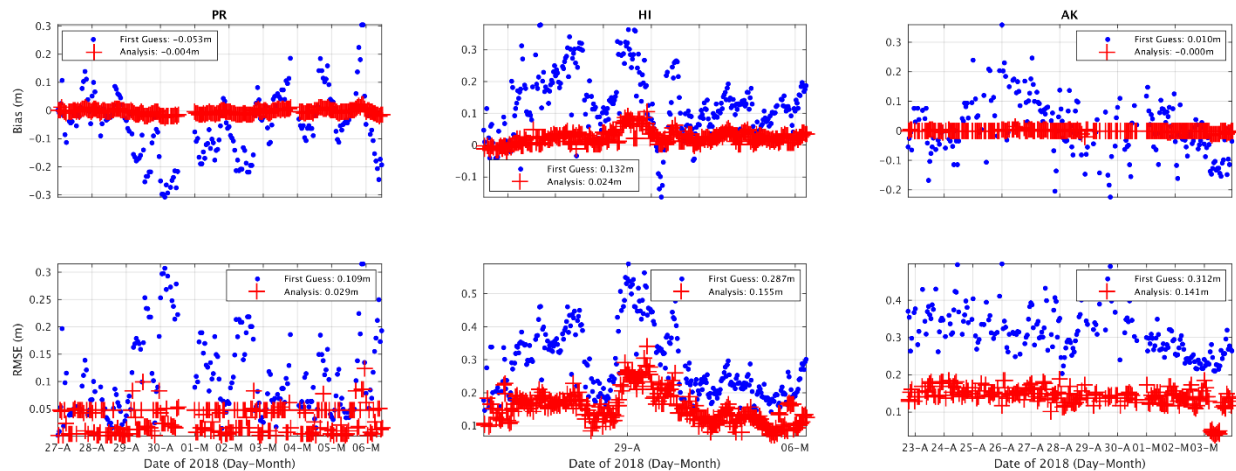


Figure 1. Time series of error statistics (top: bias, bottom: RMSE) for PR, HI and AK (from left to right), of the first guess (blue) and the analysis (red).

Summary

With the next upgrade of NCEP’s mesoscale analysis systems tentatively scheduled for the first quarter of 2019, URMA will provide analysis of SWH for most domains of the NWS (CONUS, AK, HI and PR) and it will satisfy a long-awaited request by forecasters and others stakeholders. As the first effort in wave data analysis at NCEP, major operational components were upgraded to achieve these results from the URMA. These upgrades include the standardization of the wave data streams and modifications to the core of the GSI and to the pre- and post-processing of the URMA.

For all the domains, the difference between the analysis and observations was significantly decreased in comparison with the difference of the background field from the observations. The average bias is in principle 0 m and the RMSE is reduced more than 50 percent, lying at the order of the observations’ uncertainty. The limiting factor for increasing the accuracy of the analysis is the lack of observations and the location of the existing observations especially for the smaller domains (HI and PR), where satellite observations are less frequent.

By adding the SWH to URMA, the main benefit for the research and operational communities is the development of a complete and transferable methodology for the analysis of SWH. Additional benefits include that it is based on publicly available, community software, follows well laid out steps, has undergone extensive testing in four different operational configurations, and is relatively computationally efficient.

References

- [1] Ponca M., G. Manikin, G. DiMego, S. Benjamin, D. Parrish, J. Purser, W.-S. Wu, J. Horel, D. Myrick, Y. Lin, R. Aune, D. Keyser, B. Colman, G. Mann, and J. Vavra, 2011: The Real-Time Mesoscale Analysis at NOAA’s National Centers for Environmental Prediction: Current Status and Development. *Wea. Forecasting*, 26, 593–612. doi: <http://dx.doi.org/10.1175/WAF-D-10-05037.1>
- [2] Glahn, B. and D. P. Ruth, 2003: The new digital forecast database of the National Weather Service. *Bull. Amer. Meteor. Soc.*, 84, 195-201.
- [3] K. K. Gilbert, J. P. Craven, D. R. Novak, T. M. Hamill, J. Sieveking, D. P. Ruth, and S. J. Lord, 2015: An Introduction to the National Blend of global Models Project. Special Symposium on Model Postprocessing and Downscaling, Phoenix, AZ, Amer. Met. Soc., 3.1.
- [4] Carley, J. R., M. Ponca, et al. 2018. The Continued Development of the NOAA RTMA/URMA Systems. 98th American Meteorological Society Annual Meeting. Austin.
- [5] Wu, W.-S., R. J. Purser, and D. F. Parrish, 2002: Three-dimensional variational analysis with spatially inhomogeneous covariances. *Mon. Wea. Rev.*, 130, 2905–2916.
- [6] The WAVEWATCH III® Development Group (WW3DG), 2016: User manual and system documentation of WAVEWATCH III® version 5.16. Tech. Note 329, NOAA/NWS/NCEP/MMAB, College Park, MD, USA, 326 pp.
- [7] Ebisuzaki W. et al., 2017: WGRIB2; software available at <http://www.ftp.cpc.ncep.noaa.gov/wd51we/wgrib2/>.

Loop Current in Gulf of Mexico Hindcasts at Different Resolutions

Zulema D. Garraffo¹, Shastri Paturi¹, James A Cummings¹, Ilya Rivin¹, Todd Spindler¹, Hae-Cheol Kim¹, Yan Hao¹ and Avichal Mehra²

(¹)IMSG at NOAA/NWS/NCEP/EMC, College Park, MD, United States; (²)NOAA/NWS/NCEP/EMC, College Park MD, USA.
Email: zulema.garraffo@noaa.gov; phone: 301-683-3744

Introduction

Presently RTOFS (Real Time Ocean Forecast System)-Global (Mehra et al., 2015), an operational system at National Centers for Global Prediction (NCEP), produces daily ocean forecasts at 1/12° resolution in the global domain. RTOFS version 1.1's core uses the Hybrid Coordinates Ocean Model (HYCOM, Bleck 2002) at 1/12° resolution and 41 vertical hybrid layers coupled with the Los Alamos Community sea ICE (CICE) model. The model is initialized daily from analyses produced at the U.S. Naval Oceanographic Office (Metzger et al., 2014). RTOFS generates daily forecasts for 2 days in the past and 8 days in the future using NCEP atmospheric forcing.

The production at NCEP of daily ocean analyses by coupling RTOFS to the Navy Coupled Ocean Data Assimilation (NCODA) system (Cummings and Smedstad, 2013) is under development.

Simulations

We present results of daily analyses and 1-day forecasts produced for two model configurations. The first uses HYCOM+CICE cycled with NCODA 3Dvar on a Global 1/12° horizontal resolution domain, and the second uses HYCOM cycled with NCODA 3Dvar on a Gulf of Mexico 1/25° domain. The global domain uses 41 vertical hybrid layers, while the Gulf of Mexico domain uses 36 layers. Both simulations are initialized using the 1/12° NAVOCEANO hindcast valid on 31 January 2017. Daily NAVOCEANO hindcasts are used as nesting boundary conditions for the Gulf of Mexico high resolution (1/25°) model. The Gulf of Mexico simulation covers February-March 2017, while the global simulation is being advanced through 2017.

The simulations are forced with analysis quality forcing from the NOAA/NCEP Global Data Assimilation System (GDAS) for 2017.

Externally produced quality controlled data are used in this study to test the assimilation procedure, while the NCEP production of quality control (QC) ocean data is presently being developed for near real time. The observational data consists of the following: sea surface height (SSH) from the CryoSat, Jason, Sentinel, Altika altimeters; sea surface temperature (SST) retrievals from NOAA (18,19), and METOP (A,B); surface temperature from in-situ measurements (fixed and drifting buoys, ships); subsurface profiles of temperature and salinity from Argo, XBT, and CTD; and sea ice coverage from SSMI/S and AMSR2.

The 3D-VAR analysis is performed using a 24-hour update cycle with the analysis time centered on the update cycle interval. The observations are pre-processed using the following methods: altimeter sea surface height is incorporated using bi-monthly climatological relationships between SSH (dynamic height) and temperature and salinity at depth in the form of synthetic temperature and salinity profiles; SST observations are averaged to form super-observations to remove data redundancies using local correlation length scales; background error variances are computed from a 15-day time history of forecast differences using forecasts separated by a 48-hour time interval (twice the analysis update cycle). The NCODA analysis is done directly on the HYCOM horizontal grid (tri-polar for global, Mercator for Gulf of Mexico), and uses hybrid vertical coordinates valid at the analysis time.

The 3D-VAR analysis increments for temperature, salinity, velocity and layer thickness are incorporated into the forecast model using an incremental analysis update procedure. The global ice coverage analysis was incorporated through the CICE model. For the global domain, the analysis increments are inserted into the forecast model starting 3 hours earlier than the analysis time. The forecast is then issued from this balanced initial state.

Results

For the global simulation, SST and Argo float verifications show small biases; the RMS verification error of 0.5°C for SST and 0.85°C for Argo profiles are stable, with SST RMS error slightly increasing in the Northern Hemisphere summer. The global SSH for the end of July shows the main features of the ocean circulation (Figure 1).

For both resolutions, the Loop Current and extension position are in agreement with various SST analyses (NOAA-RTG, NOAA-AVHRR). The Gulf of Mexico 1/25° circulation develops a relatively more intense loop current (3-5Sv, not shown) than in the global simulation. The high resolution Gulf of Mexico simulation SST seems to reproduce the NOAA-AVHRR

SSTanalysis slightly better than the global simulation, as for the westward plume off the Loop Current (Figure 2).

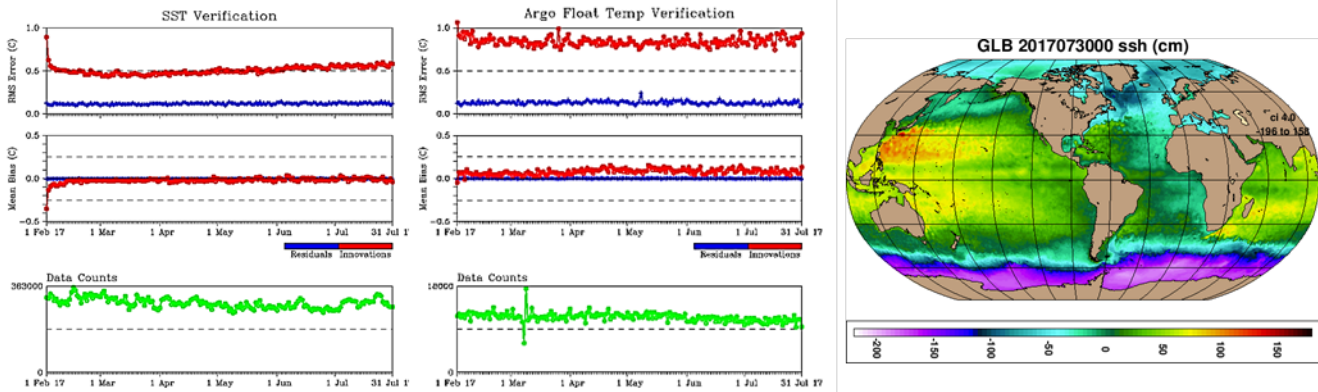


Figure 1. Left: SST verification: RMS error and mean bias, and data counts, Feb-July; center: same for Argo float temperature verification; right: SSH (1 day forecast) for July 30 2017.

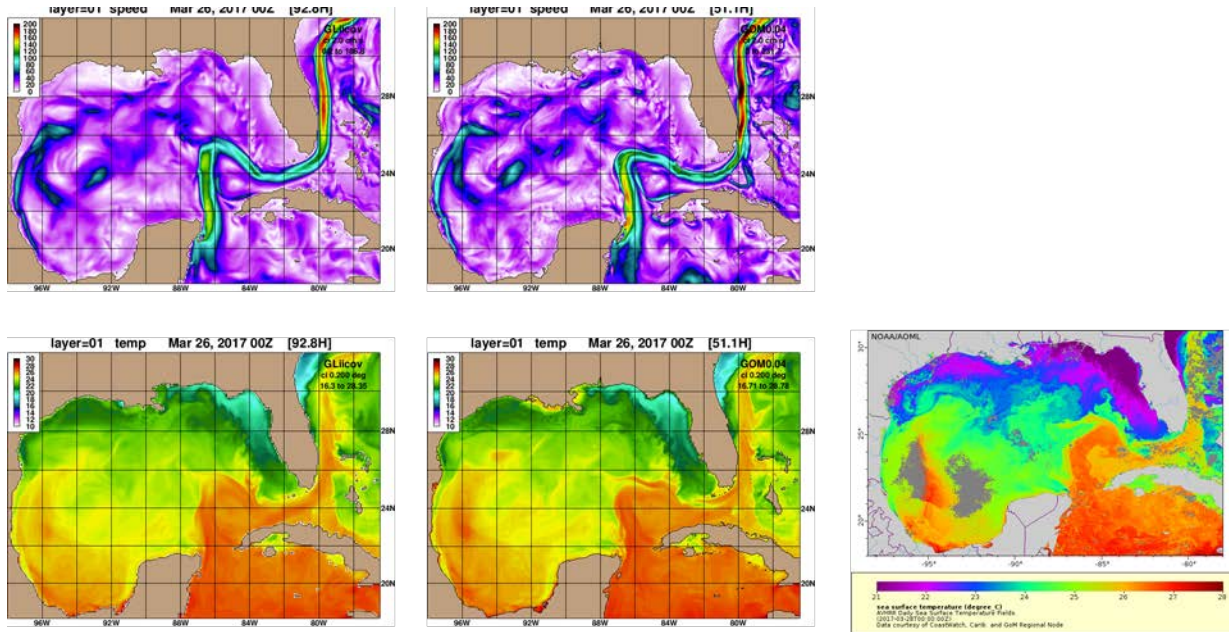


Figure 2. Top: Gulf of Mexico speed for March 26, from the global 1/12° (left) and Gulf of Mexico 1/25° (right) hindcasts. Bottom: SST (same day) from the global hindcast (left), Gulf of Mexico hindcast (center) and NOAA/AVHRR SST analysis (right)

At the end of July, the global simulation shows good agreement between the model SST and NOAA-AVHRR analysis for the Gulf of Mexico and the loop current signal (Figure 3).

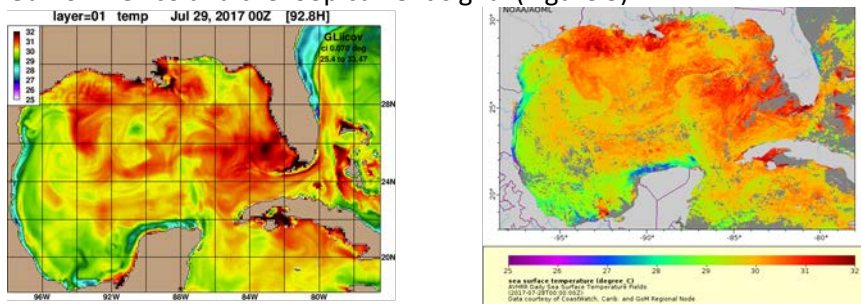


Figure 3. Left: SST from the global simulation for July 29, 2017; right: NOAA-AVHRR analysis for the same day.

References

- Bleck, R. 2002: An oceanic general circulation model framed in hybrid isopycnic-Cartesian coordinates, *Ocean Model.*, 37, 55-88.
- Cummings, J. A. and O. M. Smedstad. 2013: Variational Data Assimilation for the Global Ocean. Data Assimilation for Atmospheric, Oceanic and Hydrologic Applications vol II, Chapter 13, 303-343.
- Mehra, A.; I. Rivin; Z. Garraffo; B. Rajan, 2015. Upgrade of the Operational Global Real Time Ocean Forecast System, 2015. In: Research Activities in Atmospheric and Oceanic modeling, Ed. Askathova, WMO/World Climate Research Program Report No.12/2015. http://bluebook.meteoinfo.ru/uploads/2015/individual-articles/08_Mehra_Avichal_et al_RTOFS_Upgrade.pdf
- Metzger, E.J; O.M. Smedstad; P.G. Thoppil; H.E. Hurlburt; J.A. Cummings; A.J. Wallcraft; L. Zamudio; D.S. Franklin; P.G. Posey; M.W. Phelps; P.J. Hogan; F.L. Bub; and C.J. DeHaan, 2014. US Navy Operational Global Ocean and Arctic Ice Prediction Systems. *Oceanography* 27(3):32-43 <http://dx.doi.org/10.5670/oceanog.2014.66>

Comparisons of Two Biogeochemical Models Embedded in Hybrid Coordinate Ocean Model (HYCOM) Based Global Ocean Circulation Model

Hae-Cheol Kim^{1,*}, Carlos Lozano², Avichal Mehra², Zulema Garraffo¹

¹IMSG at NWS/NCEP/EMC, ²NWS/NCEP/EMC, ³NESDIS
Email: Hae-Cheol.Kim@noaa.gov; Phone: 301-683-3700

The NOAA Ecological Forecasting Roadmap (EFR) for 2015-2019 states that its objective is “to provide dependable, higher quality forecast products, derived from the successful transition of research and development into useful applications....” In support of this NOAA-approved roadmap, this project proposes to evaluate different approaches to develop a prototype foundational global biogeochemical model within NOAA’s global operational Real-Time Ocean Forecast System (RTOFS-Global) [1] to reliably provide the global modeling fields required to support ecological forecasts designed by EFR technical teams in a modular and expandable fashion. In particular, the objective is to establish a component for the national ocean modeling ‘backbone’ that will generate global predictions of physical and biogeochemical (BGC) variables of interest in ecological assessments (e.g., temperature, nutrients phytoplankton, oxygen, carbon and Chl-a) on a regional scale, which would enable regional applications to include the broader global context (forcings and fluxes) in their local/regional use.

In this study, using combinations of 1) the HYbrid Coordinate Ocean Model (HYCOM), ocean modeling component of the RTOFS-Global and 2) a multi-component BGC model [2][3], we present preliminary results from a series of numerical experiments run for the global domain. Within the context of NOAA’s on-going Ecological Forecasting Roadmap (EFR) efforts, we are also considering the suitability, at short- to mid-range time scales, of the proposed approaches for building biogeochemical data assimilation capabilities into the current operational system.

The HYbrid Coordinate Ocean Model (HYCOM; GLBb0.08 hereafter) with cylindrical (78.64°S – 66°S); recti-linear coordinate (66°S – 47°N); and an Arctic bipolar patch (>47°N) is used. HYCOM has 1/12-th degree horizontal resolution and 41 vertical coordinates employing hybrid layers following isopycnals in the deep sea, z-levels near the surface and terrain-following σ -coordinates in the coastal areas [4]. K-Profile Parameterization (KPP) [5] is used as a vertical mixing scheme. GLBb0.08 is forced by hourly atmospheric fluxes from NOAA’s Global Data Assimilation System (GDAS).

Two experiments are configured with different minimal complexity in biogeochemical governing equations: 1) the Nutrient-Phytoplankton-Zooplankton (NPZ) model [2]; and 2) the Nutrient-Phytoplankton-Zooplankton-Detritus (NPZD) model [3]. Figure 1 presents schematic diagrams of the two different BGC models. The major difference between the two includes the number of state equations that can simulate low-trophic level BGC components. The NPZD model includes detritus to more realistically parameterize cycling of organic particulate matter back to the dissolved inorganic nutrients’ pool. In general, due to their small number of state variables, simple models such as NPZ or NPZD have advantages in parameterization, initialization and validation of the internal ecosystem dynamics with standard and commonly available biogeochemical oceanographic measurements (e.g., chlorophyll, nutrients, zooplankton biomass). This reduces uncertainties and computational costs significantly compared to other available complex models. However, even with the small number of state variables, the parameterization and validation of marine ecological processes sometimes remain challenging if

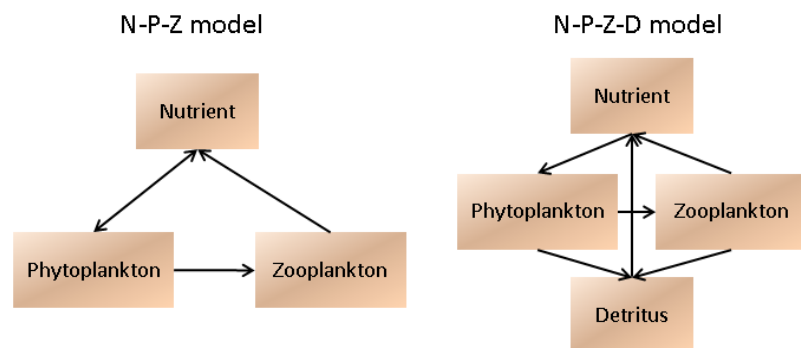


Figure 1. Schematic diagrams of the N-P-Z model (left) and N-P-Z-D model (right).

observations are sparse and incomplete. In addition, the simple models also have limitations in representing complicated ecosystem structure and functions of the real ocean that require additional measurements or experiments. This may render them less realistic, but overall, simple models are still sufficient to simulate a wide range of ecosystem phenomena.

All simulations presented here were initialized at February 1, 2017 with the HadOCC monthly mean. Model initialization for physical variables is based on the previous runs from RTOFS-Global and initial conditions for the BGC variables (e.g., lower trophic level components) are obtained from the Hadley Ocean Carbon Cycle Model (HadOCC) [6] for a realistic initialization. The simulation period is 20 days. Figure 2 presents examples of sea surface height (SSH), nitrate (NO_3^-) and phytoplankton concentration for the two numerical experiments. As tracers are not designed to influence physical properties, sea surface height (SSH) structure is identical between the two model simulations, whereas there is a noticeable discrepancy in the distribution of nitrate and phytoplankton, presumably due to varying ecosystem dynamics between the two models. Further investigations are planned for the future.

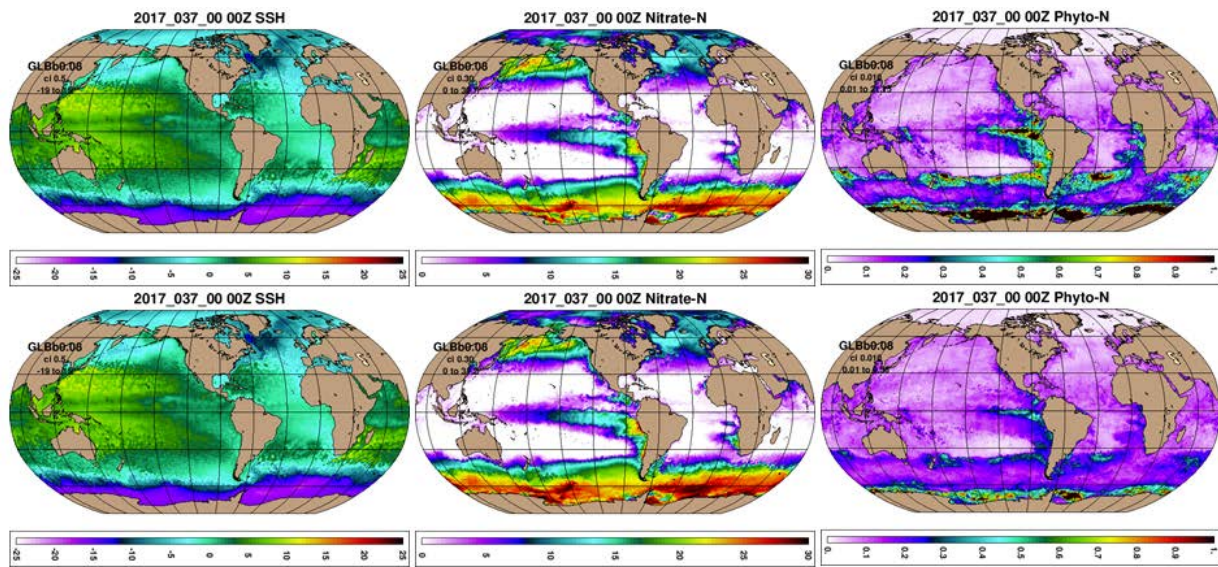


Figure 2. Comparisons between NPZ (top) and NPZD model (bottom) for sea surface height (1st column), nitrate nitrogen (2nd column), and phytoplankton nitrogen (3rd column). These snapshots are taken at 5 days (February 5, 2017) after model initialization.

[1] Mehra, A. and I. Rivin, 2010. A real time ocean forecast system for the north Atlantic Ocean. *Terr. Atmos. Ocean. Sci.* 21, 211-228

[2] Franks, P.J.S., J.S. Wroblewski and G.R. Flierl, 1986. Behavior of a simple plankton model with food level accumulation by herbivores. *Mar. Biol.* 91, 121-129.

[3] Lima, I.D., D.B. Olson and S.C. Doney, 2002. Biological response to frontal dynamics and mesoscale variability in oligotrophic environments: Biological production and community structure. *J. Geophys. Res.* 107, 10.1029/2000JC000393

[4] Bleck, R., 2002: An oceanic general circulation model framed in hybrid isopycnic-Cartesian coordinates, *Ocean Model.* 37, 55-88.

[5] Large, W.C., J.C. McWilliams and S.C. Doney, 1994: Oceanic vertical mixing: a review and a model with a nonlocal boundary layer parameterization. *Rev. Geophys.* 32, 363-403.

[6] Ford, D.A., K.P. Edwards, D. Lea, R.M. Barciela, M.J. Martin and J. Demaria, 2012. Assimilating GlobColour ocean colour into a pre-operational physical-biogeochemical model. *Ocean Sci.* 8, 751-771.

Assimilation of science-quality ocean color products from Visible Infrared Imager Radiometer Suite (VIIRS) into Hybrid Coordinate Ocean Model (HYCOM)

Hae-Cheol Kim^{1,*}, James Cummings¹, Zulema Garraffo¹, Avichal Mehra², Eric Bayler³, Shastri Paturi¹

¹IMSG at NWS/NCEP/EMC, ²NWS/NCEP/EMC, ³NESDIS/STAR

Email: Hae-Cheol.Kim@noaa.gov; Phone: 301-683-3700

Recent advances in biogeochemical (BGC) models and data collection programs with greater spatio-temporal coverage make it possible “to predict and assess trends of marine biogeochemical cycles and to safeguard marine ecosystems” [1]. Implementation of various data assimilation (DA) schemes for the National Center for Environmental Prediction (NCEP) operational Real-Time Ocean Forecast System (RTOFS-Global), along with data streams of real-time/near-real-time physical, biological, and chemical data allow the analysis and forecasting of global BGC states. The main motivation of this study, funded by Joint Polar Satellite System (JPSS) - Proving Ground and Risk Reduction (PGRR) Program at NOAA’s National Environmental Satellite, Data, and Information Service (NESDIS), is to demonstrate how various satellite ocean color products can be used in a global ocean modeling framework.

This study presents preliminary results from a series of numerical experiments run for a Gulf of Mexico testbed, exploring combinations from: 1) science-quality ocean color products from the Visible Infrared Imager Radiometer Suite (VIIRS) on the Joint Polar Satellite System (JPSS); 2) the HYbrid Coordinate Ocean Model (HYCOM), the ocean modeling component of the RTOFS; 3) a 3-component Nutrient-Phytoplankton-Zooplankton (NPZ) model [2]; and 4) the NOAA version of the Navy Coupled Ocean Data Assimilation (NCODA) system [3]. Within the context of NOAA’s on-going Ecological Forecasting Roadmap (EFR) efforts, we examine the suitability, at short- to mid-range time scales, of the proposed approaches for building biogeochemical data assimilation capabilities into the current operational system.

The global HYCOM (GLBb0.08 hereafter), with recti-linear coordinates (66°S – 47°N) and an Arctic bipolar patch (>47°N), is used. This HYCOM has 1/12-th degree horizontal resolution and vertical coordinates employing 41 layers, following isopycnals in the deep sea, z-levels near the surface, and terrain-following σ -coordinates near coastal areas [4]. K-Profile Parameterization (KPP) [5] is used as the vertical mixing scheme. GLBb0.08 is forced by hourly atmospheric fluxes from NOAA’s Global Data Assimilation System (GDAS). For this effort, the Gulf of Mexico (GOMI0.04) is selected as the testbed for various DA numerical experiments. GOMI0.04 has 1/25-th degree horizontal resolution and vertical coordinates with 36 layers following isopycnals. For a realistic initialization, the physical state variables are initialized with the previous run of RTOFS-Global, with the initial conditions for the BGC variables (NPZ concentrations) being obtained from the Hadley Ocean Carbon Cycle Model (HadOCC) [6].

The NCODA system is an oceanographic implementation of the three-dimensional variational (3DVAR) technique. NCODA 3DVAR, a unified and flexible oceanographic analysis system (Figure 1), is transitioning to NCEP for operational use as the data assimilation component for RTOFS-Global. The analysis variables include temperature, salinity, geopotential (dynamic height), u , v vector velocity components, and chlorophyll concentration from ocean color products. All ocean variables are analyzed simultaneously in three dimensions. The horizontal correlations are multivariate in geopotential and velocity, thereby permitting adjustments to the mass fields to be correlated with adjustments to the flow fields.

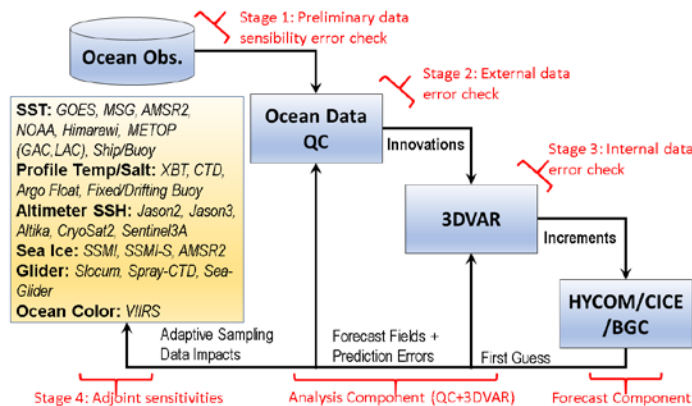


Figure 1. A schematic diagram of ocean data assimilation in the NCODA system. Note that oceanographic and satellite data products are available as of 2018.

The velocity adjustments (or increments) are in geostrophic balance with the geopotential increments, which, in turn, are in hydrostatic agreement with the temperature and salinity increments. The chlorophyll assimilation is used to constrain the BGC properties of the ocean in the NPZ model. Two experiments are made: 1) a free mode with no data assimilation; and 2) a data-assimilative mode. For data assimilation, only physical oceanographic data from various platforms (e.g., satellite sea-surface height anomalies, satellite sea-surface temperatures, temperature and salinity profiles, etc) were assimilated. All simulations were initialized at February 1, 2017, with, as previously mentioned, physical state variables being restarted with RTOFS-Global simulations and BGC state variables being initialized with HadOCC model output. The simulation period is 20 days. Figure 2 presents examples of sea surface height (SSH), nitrate (NO_3^-), and phytoplankton concentration for the free and data assimilative modes 10 days after initialization. It is noteworthy that the SSH structure becomes slightly different between the two simulations, which is also true for the BGC tracers. There are subtle discrepancies in the distributions of nitrate and phytoplankton, presumably due to changes in mesoscale eddy features. More investigation is required.

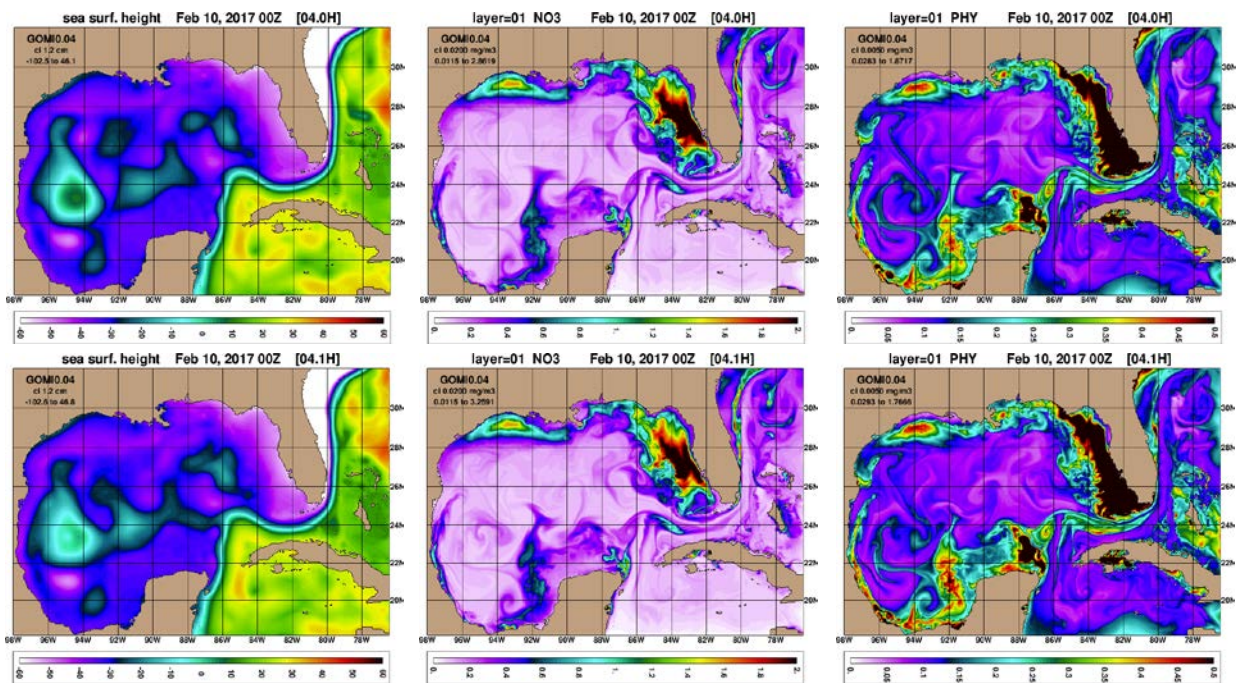


Figure 2. Comparisons between free (top) and data-assimilative runs (bottom) for sea surface height (1st column), nitrate nitrogen (2nd column), and phytoplankton nitrogen (3rd column).

- [1] Brasseur, P., N. Gruber, R. Barciela, K. Brander, M. Doron, A. El Moussaoui, A.J. Hobday, M. Huret, A.-S. Kremer, P. Lehodey, R. Matear, C. Moulin, R. Murtugudde, I. Senina, and E. Svendsen., 2009. Integrating biogeochemistry and ecology into ocean data assimilation systems. *Oceanography* 22(3):206–215, <http://dx.doi.org/10.5670/oceanog.2009.80>.
- [2] Franks, P.J.S. , J.S. Wroblewski, and G.R. Flierl, 1986. Behavior of a simple plankton model with food level accumulation by herbivores. *Mar. Biol.* 91, 121–129.
- [3] Cummings, J.A. and O.M. Smedstad, 2013. Variational data assimilation for the global ocean. In: S.K. Park and L. Xu (Eds.), *Data Assimilation for Atmospheric, Oceanic and Hydrologic Applications Vol. II.*, doi: 10.1007/978-3-642-35088-7_13, Springer-Verlag, Berlin Heidelberg.
- [4] Bleck, R., 2002: An oceanic general circulation model framed in hybrid isopycnic-Cartesian coordinates, *Ocean Model.*, 37, 55-88.
- [5] Large, W.C., J.C. McWilliams and S.C. Doney, 1994: Oceanic vertical mixing: a review and a model with a nonlocal boundary layer parameterization. *Rev. Geophys.* 32, 363-403.
- [6] Ford, D.A., K.P. Edwards, D. Lea, R.M. Barciela, M.J. Martin, and J. Demaria, 2012. Assimilating GlobColour ocean colour into a pre-operational physica-biogeochemical model. *Ocean Sci.* 8, 751-771.

Nonlinear Wave Ensemble Averaging using Neural Networks

Vladimir Krasnopolsky¹, Ricardo Martins Campos², Jose-Henrique Alves³, Stephen Penny²

¹EMC/NCEP / NOAA Center for Weather and Climate Prediction

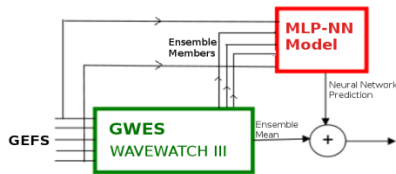
²Dept. of Atmospheric & Oceanic Science / University of Maryland

³SRG/EMC/NCEP / NOAA Center for Weather and Climate Prediction

e-mail: vladimir.krasnopolsky@noaa.gov

1. Introduction

An experiment applying neural networks (NNs) to nonlinear wave ensemble averaging is conducted in the Gulf of Mexico (GOM). It is an approach that expands the traditional arithmetic ensemble mean (EM) to a nonlinear mapping that better captures the differences among the ensemble members. The NNs have the members of the Global Wave Ensemble System (GWES) as input, and NN outputs are trained using six NDBC buoys (42001, 42002, 42003, 42039, 42055, 42360). The variables selected for the study are 10-m wind speed (U10), significant wave height (Hs), and peak period (Tp) for the year of 2016. The first experiments testing NN architectures for GWES nonlinear wave ensemble averaging at single locations were reported by Campos et al. (2017). It was found that the best NN model was composed of two layers with 11 neurons at the intermediate layer, using a basis function of the hyperbolic tangent, sequential training, and the log function applied to time series of significant wave height. Equation 1 shows the final strategy of the NN simulation, where the simple arithmetic EM is first calculated and then the NN model is applied to model the residue (difference between the target value and EM). This method can focus the NN simulation on the nonlinear part, instead of simulating the whole signal with linear and nonlinear components (Krasnopolsky, 2013). It builds a more robust model that provides reliable ensemble averages at different metocean conditions and sea severities.



$$NEM = EM + NN_r(p_1, p_2, \dots, p_n) \quad (1)$$

2. Neural Network training and sensitivity tests

At each particular grid point, the inputs of the NN consisted of 63 ensemble members (20 ensembles plus one control member, for U10, Hs, and Tp) plus the sine and cosine of time (to capture seasonality effects). To introduce space in the NN model, latitude and longitude were included for a total of 67 inputs. In order to determine the complexity of the NN model required to obtain the optimal training, architectures with 12 different numbers of neurons, 8 different filtering windows (time-domain), and 100 seeds for the random initialization were studied. We constructed different NNs for specific forecast days, from Day 0 to Day 10. The number of neurons and filtering windows (hours) using the moving average method are, respectively, $N [2, 5, 10, 15, 20, 25, 30, 35, 40, 50, 80, 200]$ and $FiltW [0, 24, 48, 96, 144, 192, 288, 480]$ hours. Two thirds of the available data was selected for training and 1/3 for the test set, using a cross-validation scheme with 3 cycles.

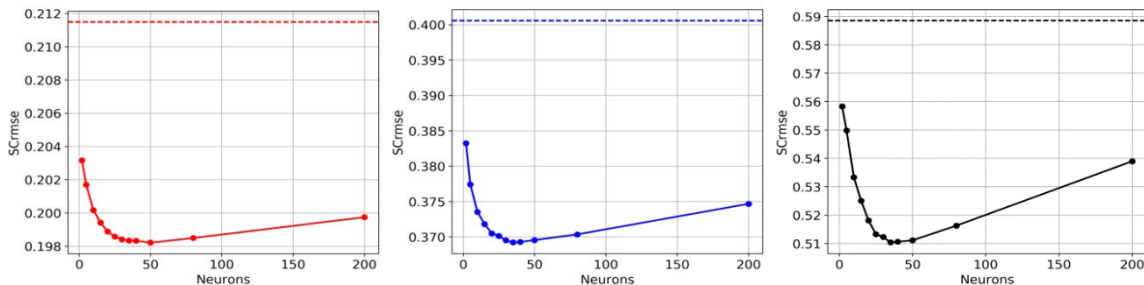


Figure 1 – Scatter component of the RMSE (SC_{rmse}) obtained for the NN training tests on forecast Day 0 (red), Day 5 (blue), and Day 10 (black) for significant wave height Hs. Results involving different initializations and filtering windows were averaged to analyze the sensitivity to the number of neurons only. The solid line is the NN model results while the dashed line is the result for the ensemble mean (EM); shown to compare their performances. Points at the plots represent the number of neurons equal to 2, 5, 10, 15, 20, 25, 30, 35, 40, 50, 80, and 200.

Results obtained show that the bias is not very sensitive to the number of neurons so a few neurons are sufficient to improve the bias; however, the scatter error is highly sensitive to the number of neurons (Figure 1). The scatter component of the RMSE (SC_{rmse} , Mentaschi et al., 2013) and the correlation coefficient (CC) are continuously improved by higher number of neurons; however, when the number of neurons approaches 40 to 50 neurons the results start deteriorating. Regarding the filtering window, optimum results were found between 48 to 192 hours; which is mainly because the moving average filtering removes high frequency noise from the signal which helps the NN to minimize the scatter error. The best NN configuration for each forecast day was independently selected for the final simulations and assessments. The first row of Figure 2 shows two significant improvements. The first is the benefit of the NCEP ensemble approach of GWES, indicating that the arithmetic ensemble mean has better skill than the control run. The second is the further improvement provided by the nonlinear ensemble averaging using NNs. Both are more evident at longer forecast times.

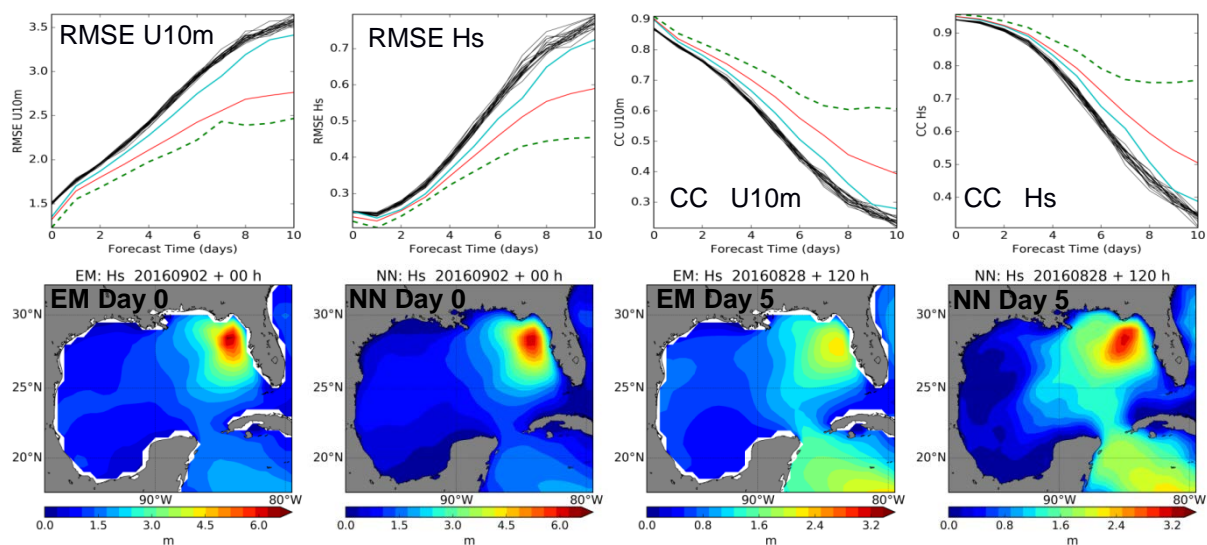


Figure 2 – RMSE and CC as a function of forecast time for U10 and Hs, at the top row, where the black curves are the GWES members, cyan is the deterministic (control) run, red the arithmetic ensemble mean (EM), and green the nonlinear ensemble averaging using NNs. The bottom row shows the maps of Hs related to Sep/02/2016 00Z (Hurricane Hermine), with different forecast times.

3. Conclusions

Our results show that using NN models demonstrates their main advantages at longer forecast times. Although the NNs do not deal with physical aspects, the improvement of the NN experiment is not restricted to one variable, but the U10, Hs, and Tp have all benefited. It was verified that the conservative ensemble approach (EM) is excellent in reducing the scatter component of the errors but it does not improve the systematic bias, as was expected. The NN experiment described was able to reduce the systematic errors as well as the scatter error, proving to be a useful tool not only for bias correction but also to significantly improve the whole forecast. Error metrics applied to all variables and forecast ranges indicated that, apart from the bias of U10 in the Day-10 simulations, all the results using NNs proved to be better than the arithmetic mean (EM). The GOM maps of Figure 2 present an example for Hurricane Hermine, when the NNs better captured the extreme event than EM, especially at Day 5.

References

- Campos, R.M., Krasnopolsky, V., Alves, J.-H., Penny, S., 2017, Improving NCEP's Probabilistic Wave Height Forecasts Using Neural Networks: A Pilot Study Using Buoy Data. National Oceanic and Atmospheric Administration - Office Note 490, <http://doi.org/10.7289/V5/ON-NCEP-490>
- Krasnopolsky, V., 2013. "The Application of Neural Networks in the Earth System Sciences. Neural Network Emulations for Complex Multidimensional Mappings", Springer, 200 pp.
- Mentaschi, L., Besio, G., Cassola, F., Mazzino, A., 2013. Problems in RMSE-based wave model validations. Ocean Modelling, 72, 53–58.

Using a Neural Network Model Coupled to a Real-Time Ocean Forecast System for Short-Term Ocean Color Predictions

Sudhir Nadiga¹, Vladimir Krasnopolsky², Avichal Mehra², Eric Bayler³,
Shastri Paturi¹, Zulema Garraffo¹, Hae-Cheol Kim¹, and Ilya Rivin¹

¹IMSG at NOAA/NWS/NCEP/EMC, ²NOAA/NWS/EMC, ³NOAA/NESDIS/STAR

In this paper, a Neural Network (NN) model using vertical profiles (0-200m) of temperature, salinity, and zonal velocity and sea surface height fields from the operational Real-Time Ocean Forecast System (ROTFS; Mehra, *et al*, 2011) is used to produce short-term global ocean color (OC: chlorophyll-a and KdPar) forecasts. The underlying scientific premise of this NN model is that ocean color fields — signatures of ocean biological processes — can be statistically correlated to upper ocean physical states. The NN model is trained over many months (July 2013 to December 2015) using NOAA Visible Infrared Imaging Radiometer Suite (VIIRS) science-quality ocean color fields and RTOFS inputs. Then the trained NN model is used for ocean color predictions for an independent data set from 2016. The purpose of this preliminary study is to test the suitability of this coarse-resolution NN model: (a) for initiating global ocean color predictions, (b) as a proof-of-concept for the NN model configuration, and (c) as a test case for embedding the NN ocean color model in future versions of the coupled seasonal forecasting system. As shown in Figures 1 and 2, the coarse-resolution NN model is able to successfully predict the OC fields over most of the tropical oceans, but there are many regions in the global oceans where the NN model has significant issues.

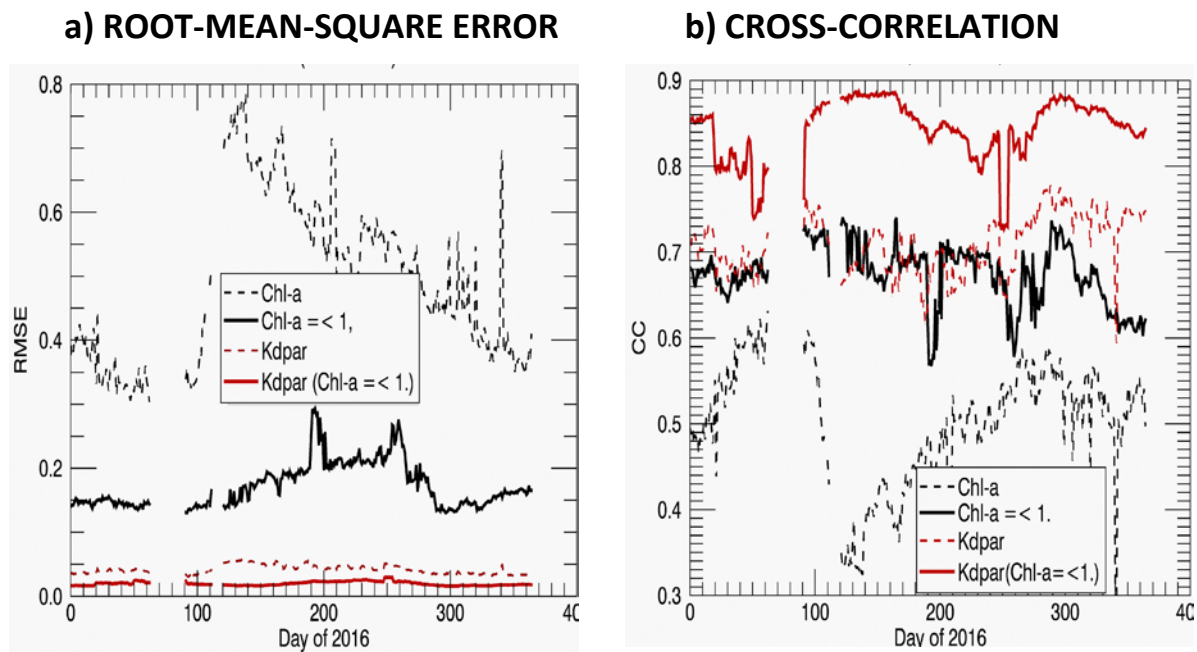
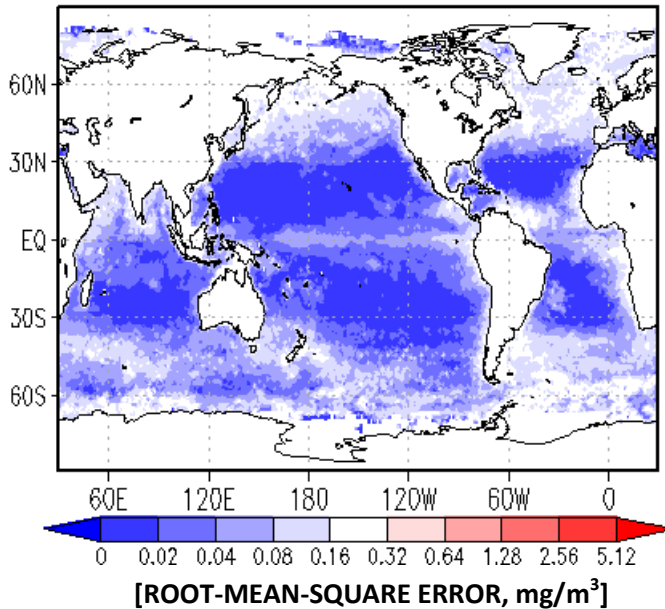


Figure 1: Time-Series plots of: (a) global root-mean-square error, and (b) global cross-correlation for Neural Network daily chlorophyll-a and kdpar predictions for 2016.

a) ROOT-MEAN-SQUARE ERROR



b) CROSS-CORRELATION

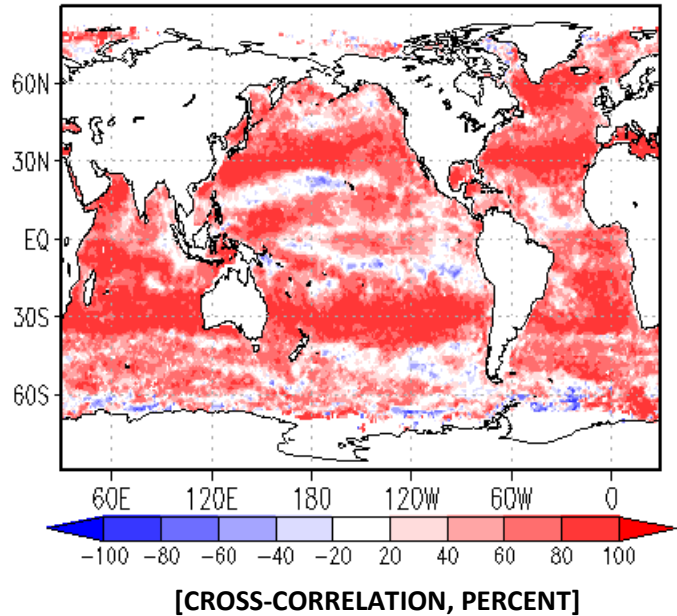


Figure 2: Spatial plots of: (a) root-mean-square error (mg/m^3), and (b) cross-correlation (percent) for Neural Network daily chlorophyll-a predictions for 2016.

In this coarse-resolution proof-of-concept, the 1/12-degree RTOFS inputs and 4-Km VIIRS ocean color fields were collocated into $1^\circ \times 1^\circ$ resolution for July 2013-December, 2016. The test set spans 07/5/2013 to 12/31/2015; and the validation set is from 1/1/2016 to 12/30/2016. While the NN provides excellent results over many oceanic domains, there are significant errors over the continental shelves and the oligotrophic subtropical gyres, where the signal-to-noise ratio is low with low potential predictability. Also, the NN performs significantly better for kdpar than for chlorophyll-a and for low values of chlorophyll-a. These results are similar to that shown in Nadiga, *et al.* (2015) and Krasnopolsky, *et al.*, (2017). The expected NOAA users of this new potential capability are NCEP, for improved ocean and coupled modeling (incorporating 2-way coupling to account for biological variability in weather/climate system), NMFS, for gap-filled ocean color predictions in fisheries monitoring, and NOS, for ocean color boundary conditions for coastal /estuarine modeling.

References:

- Mehra et al. (2011) A Real Time Operational Global Ocean Forecast System. US GODAE Ocean View Workshop on Observing System Evaluation and Intercomparisons, Univ. of California Santa Cruz, CA, USA, 13-17 June 2011.(available at http://polar.ncep.noaa.gov/global/about/GODAE11_poster_d1.pdf)
- Nadiga, S., Krasnopolsky, V., Mehra, A., Bayler, E., and Behringer, D., Neural Network Technique for Gap-Filling of Satellite Ocean Color Observations for Use in Numerical Ocean Modeling, Poster 106, 2nd International Ocean Colour Science Meeting, San Francisco, CA, 2015.
- Krasnopolsky, V., Nadiga, S., Mehra, A., Bayler, E., and Kim, H.-C., Optimization of a Neural Network-Based Biological Model for Chlorophyll-a Concentrations in the Upper Ocean, NCEP Office Note, 487, 2017.

Annual and Semiannual Cyclicity of the Upper Ocean Temperature from Model Simulations

B.S. Strukov, and Yu.D. Resnyanskii

Hydrometeorological Research Centre of Russian Federation (bsstr@mail.ru)

1. Introduction

The most pronounced temporal changes of the thermal state of the upper ocean in middle and high latitudes are determined by the seasonal course of solar insolation and have an annual period. In some areas of the ocean, in addition to the annual cycle, higher harmonics may also be present. Harmonics of this kind having a half-year period were examined, for example, in [1] basing on processing the Argo observations. Here we are trying to trace the geography of such oscillations, their origin and mode structure using the simulations with the NEMO model.

2. Model configuration

For the analysis, the simulations with Version3.6 of the NEMO model [3], coupled with the ice model LIM3, were used. The simulations were performed with a one-degree horizontal resolution and 75 vertical levels ($362 \times 332 \times 75$ grid-points). The atmospheric forcing at the ocean surface was prescribed from the DFS5.2 data set [2]. During the model integration, the observational data from profiling Argo buoys were assimilated through the 3Dvar analysis and the computed sea ice concentrations were corrected by satellite observations using the nudging technique. The model output was averaged over 5 day intervals during overall simulation period 01.01.2001–31.12.2010.

3. Geographical features of annual and semiannual cyclicity

Figure 1a shows the frequency spectra of the upper ocean temperature fluctuations, obtained from the 01.01.2001–31.12.2010 simulation, and Figures 1b and 1c are the geographical distributions of the amplitudes of annual and semiannual oscillations. The amplitudes were evaluated as the coefficients of Fourier expansion.

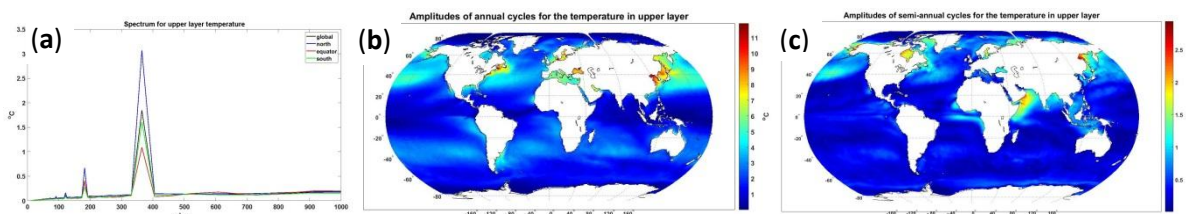


Figure 1. (a) Frequency spectra of the upper ocean temperature fluctuations for the global World Ocean (black), Northern Hemisphere (blue), Southern Hemisphere (green) and equatorial region (red). (b) and (c) The amplitudes of annual and semiannual oscillations correspondingly.

As is seen from the Figure, the annual oscillations are most pronounced in the Northern Hemisphere, especially in the western parts of the oceans. This can be obviously explained by the influence of air masses carried from the continent regions by western winds and characterized by enhanced seasonal variations typical for continental climate conditions. The predominance of land over the ocean area in the Northern Hemisphere also explains the greater amplitude of annual fluctuations as compared with those in the Southern Hemisphere.

In the near equatorial region, annual changes are less pronounced, and proportion of semi-annual fluctuations increases. The both amplitude distributions in Figures 1b and 1c are generally similar to those obtained by Chen and Wang [1] from direct processing of Argo data. This similarity may be considered as a confirmation of consistency of the model results with observations.

The semiannual components of the spectrum are of different origin in different regions. For example, in the Indian Ocean, the semiannual harmonic is generated by monsoonal processes with half year periodicity [4]. As is seen from Figure 2a, in the western part of the Arabian Sea this

harmonic corresponds to real oscillations with half year period. In contrast to this, in regions with water temperature remaining for some time near the freezing point during winter season the semiannual harmonic is just an artifact of the annual changes differing in form from sinusoidal (Figure 2b). It can be assumed that the actual semiannual nature of temperature fluctuations occurs in places where the ratio of the amplitudes of the semiannual component to the annual one is comparable to or greater than one. This takes place in the near equatorial belt (Figure 2c).

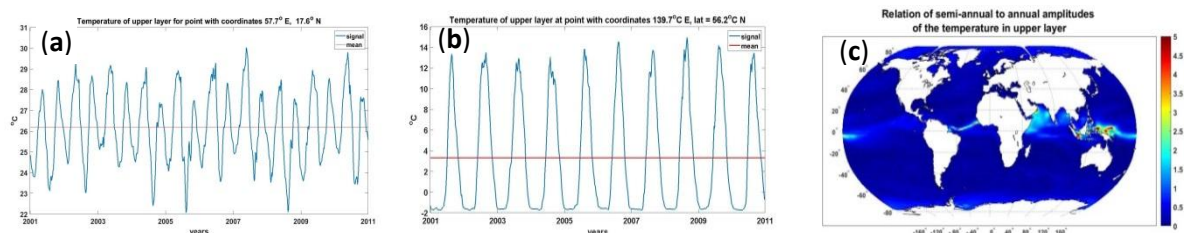


Figure 2. Temporal changes of the upper ocean temperature in the western part of the Arabian Sea (a), in the western part of the Sea of Okhotsk (b) and geographical distribution of the ratio of the amplitudes of semiannual and annual harmonics (c).

4. Modal structure

The semiannual cycle may also be traced in the EOF coefficients (Figure 3). The EOFs (empirical orthogonal functions) and expansion coefficients were computed using as input model time series from which the annual changes were filtered out. Calculated in this way the first EOF mode characterizes to semiannual changes, and the second mode characterizes oscillations with periods of 4–5 years. However, in order to obtain more reliable estimates of such oscillations, longer simulations are required, which are planned to be performed in the near future.

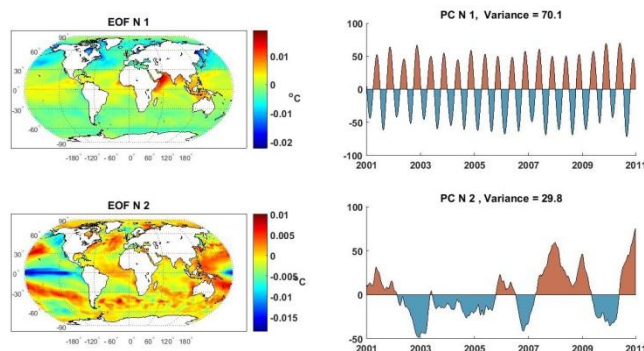


Figure 3. The geography of the first and second EOF modes of the upper ocean temperature with filtered seasonal changes (left panels) and the corresponding expansion coefficients for 01.01.2001–31.12.2010 (right panels).

References:

1. Chen, G., and X. Wang, 2016: Vertical structure of upper-ocean seasonality: Annual and semiannual cycles with oceanographic Implications. *J. Climate*, **29**, 37–59, doi: 10.1175/JCLI-D-14-00855.1
2. Dussin, R., B. Barnier, L. Brodeau, and J.M. Molines, 2016: The Making of the DRAKKAR FORCING SET DFS5. DRAKKAR/MyOcean Report 01-04-16. April 2016. –34 p. https://www.drakkar-ocean.eu/publications/reports/report_DFS5v3_April2016.pdf.
3. Madec, G. and the NEMO team. 2015: NEMO ocean engine. Version 3.6 stable. November 2015. ISSN No 1288-1619. –391 pp. http://www.nemo-ocean.eu/About-NEMO/Reference-manuals/NEMO_book_3.6_STABLE.
4. Skripaleva, E.A., 2009: Features of seasonal variability of the Indian Ocean surface temperature field from in situ and satellite data. *Reports of the National Academy of Sciences of Ukraine*, No 12, 126-131. (in Russian)

“Noise” generation in climatologically driven ocean models with different grid resolutions

Tang Shengquan (1, 2), Hans von Storch (1, 2) and Chen Xueen (1)

(1) Ocean University of China, Qingdao, PR China

(2) Institute of Coastal Research, HZG, Geesthacht, Germany

Email: 2277520917@qq.com, hvonstorch@web.de, xchen@ouc.edu.cn

We are testing the **hypothesis** that nonlinear-systems like ocean dynamics are generating variability by themselves without any external forcing. We examine the output of a three-layer nested numerical simulation which was performed with an almost global model with 1° grid resolution, an embedded West Pacific model (WestPac) with 0.2° grid resolution, and an embedded Southern China Sea (SCS) model with 0.04° grid resolution. The variability, which can be conceptualized as “noise”, is mostly created in the model component of higher grid resolution.

The model used is Hybrid Coordinate Ocean Model (HYCOM) that is exposed to periodic climatological atmospheric forcing, with a fixed annual cycle but without weather disturbances. The atmospheric forcing comes from the Comprehensive Ocean-Atmosphere Data set (COADS). The simulation regions are shown in Figure 1 (see Tang et al., 2018). We analyzed daily averages for every layer model over a 21-year period.

We measure the amount of variability by the variance of daily values (centered on the long-term monthly means) at each grid point. The variable considered is the daily barotropic stream function (BS). The maps in Figure 2 show the spatial distributions of the logarithm of BS variances in the SCS in two seasons (summer and winter monsoon) simulated by three models (global, West-Pacific and South China Sea). Table 1 lists the daily BS variances averaged across the SCS.

The variances in the WestPac are somewhat increased compared to the global run; for the SCS-simulation we find substantially larger variances. We propose that the models ability to generate eddies in the South China Sea is the main cause for the increase in variability.

Our experiments support the concept that dynamical models of the ocean generate internal, unprovoked variability. This “noise” generation is stronger in models with higher resolution. Indeed such behavior is to be expected from the “stochastic climate model” (Hasselmann, 1976). This noise represents for certain issues a nuisance (hiding real effects of forcing) but is also constitutive for the dynamical properties of the system (von Storch et al., 2001). “Noise” has significant implications for issues like “detection and attribution of climate change” and for numerical experimentation with ocean models.

Hasselmann, K., 1976: Stochastic climate models. Part I. Theory. *Tellus* 28, 473-485.

von Storch, H., J.-S. von Storch, and P. Müller, 2001: Noise in the Climate System - Ubiquitous, Constitutive and Concealing. In B. Engquist and W. Schmid (eds.) *Mathematics Unlimited - 2001 and Beyond*. Part II. Springer Verlag, 1179-1194.

Tang, S., Chen X, Zeng Z, and Zhai X, 2018: On the dynamics of SCS deep circulation: the role of surface wind and the Luzon inflow; submitted to *J. Geophys. Res.*

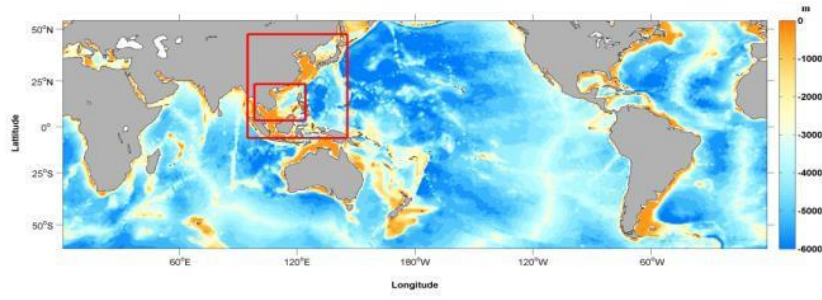


Fig. 1 The regions of the three-nested numerical simulation.

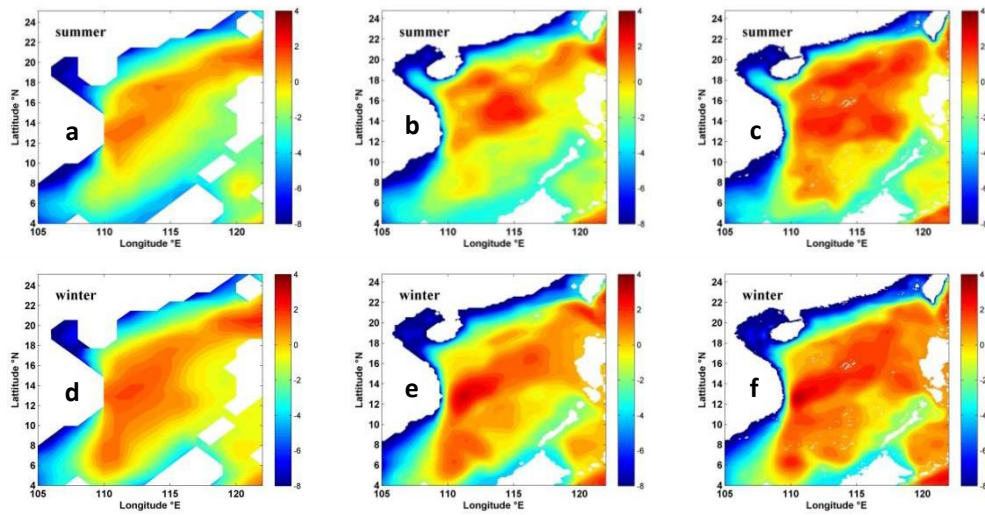


Fig.2 The spatial distributions of logarithm of BS variances in the SCS simulated by the global model (a, d), WestPac model (b, e) and the SCS model (c, f).

Table 1 The spatial averages of the daily BS variances in the SCS simulated by three models

	Global model (SV ²)	WestPac Model (SV ²)	SCS Model (Sv ²)
Spring	0.8396	1.2777	1.7187
Summer	0.5801	0.8328	1.6161
Fall	2.2413	2.5619	3.2377
Winter	1.0744	1.4574	1.9925
Year	3.2975	5.3550	6.1782